Timing parameter optimization for comparison experiments of TSIM

Hongrui Wang,[1,*] Huiduan Li,[2] and Wei Fang[1]

[1]Changchun Institute of Optics, Fine Mechanics and Physics, Chinese Academy of Sciences, Changchun 130012, China

[2]Chuxiong Normal University, Chuxiong 675000, China

*Corresponding author: wanghongrui@ciomp.ac.cn

Received 25 September 2013; revised 9 January 2014; accepted 7 February 2014; posted 7 February 2014 (Doc. ID 198273); published 11 March 2014

The optimization problem of an absolute radiometer's timing parameters is investigated for comparison experiments of Total Solar Irradiance Monitor (TSIM). Comparison experiments were performed to establish the TSIM's contact with other space radiometers for measuring total solar irradiance (TSI). Since the comparison experiments had to be performed on a tight schedule under the impact of weather conditions, the measurement parameters for the comparison experiments were selected carefully using optimized solutions of timing parameters. The optimized solutions were identified by a genetic algorithm (GA) based on a thermal model of an absolute radiometer. The thermal model includes terms of heat radiation, air conduction, etc. Fitness value function and constraints of GA are constructed using the thermal model. The experimental results indicate that the selected measurement parameters are sufficient to implement accurate calibration of TSI, providing more opportunities for solar observation.

OCIS codes: (120.0120) Instrumentation, measurement, and metrology; (120.5630) Radiometry; (280.0280) Remote sensing and sensors; (280.4788) Optical sensing and sensors.

http://dx.doi.org/10.1364/AO.53.001718

1. Introduction

Total Solar Irradiance Monitor (TSIM) is an instrument for measuring total solar irradiance (TSI). It was sent into space onboard the FY-3C polar orbiting meteorological satellite on 23 September 2013. The FY-3C satellite is the third satellite of the FY-3 (FengYun-3) [1] meteorological satellite series. TSIM/FY-3C tracks the sun in space by itself using a solar tracking subsystem. The objective of TSIM is to provide long-time continuous record of TSI to understand solar variability [2]. Two electrical substitution radiometers [3–6] AR1 and AR2 are used for TSIM/FY-3C. TSIM's traceability to the World Radiometric Reference (WRR) [7] is achieved through ground-based comparison experiments at ambient temperature and pressure. Solar Irradiance Absolute Radiometer (SIAR)-type radiometers SIAR-1a and SIAR-2c are used as transfer instruments. Comparison experiment is one step for instrument calibration [8,9], establishing TSIM's contact with other radiometers that monitor TSI simultaneously in space [10–12]. SIAR-1a and SIAR-2c have already been calibrated to WRR by the World Standard Group (WSG) TSI instruments in the 11th International Pyrheliometer Comparison (IPC-XI), 2010 [7]. Four absolute radiometers measured TSI in air and they were pointed to the sun together by a solar tracking device in the comparison experiment [13].

Comparison experiments of TSIM/FY-3B lasted for 23 days in 2009 and the FY-3B satellite is the second satellite of the FY-3 satellite series. However, the comparison experiments of TSIM/FY-3C had to be performed in 8 days to have the possibility of a

1559-128X/14/091718-09$15.00/0

launch mission. It is a challenge to get sufficient TSI measurements in such short time under the influence of weather conditions. No TSI observations are available for days of bad weather, such as rain or cloud. Accurate solar measurements should be produced as fast as possible. However, a specific time is desired for a single TSI measurement to ensure data accuracy. It is a problem to get a subtle balance between data quantity and data accuracy. And good understanding of an absolute radiometer's thermal dynamics is required. Although the thermal model of the electrical substitution radiometer had been studied for a long time [3,4,14], little literature is available on estimating the parameters of the thermal model. However, some parameters denoted as timing parameters inside the thermal model are required to be known for determining the parameters for the comparison experiments. The optimization problem of the timing parameters is investigated in this paper to achieve meaningful selection of measurement parameters for TSIM's comparison experiments.

2. TSI Measurement

The four absolute radiometers used in the comparison experiments share nearly the same design. A computer-aided design view of the radiometer SIAR-1a is shown in Fig. 1. A primary cavity and a reference cavity are used as TSI sensors [3,4]. The primary cavity is connected to a heat sink for thermal stability. A thermocouple ring is laid at the opening of the primary cavity for temperature measurement. The reference ends of the thermocouples are connected to the heat sink, whereas the measuring end of the thermocouples is connected to the wall of the primary cavity. The temperature detected by the thermocouples is the temperature difference between the heat sink and the primary cavity. The temperature detected by the thermocouples is converted to a digital signal by a 16 bit analog-to-digital (A/D) converter. A heater winding is embedded into the wall of the primary cavity for heating. The reference cavity has no heater winding and it is not exposed to sunlight. The reference cavity also has a thermocouple ring at its opening, which is connected in series to the thermocouple ring of the primary cavity to compensate for temperature drift of the heat sink. The influence of the heat sink's temperature drift is nearly canceled by the configuration of the dual cavity.

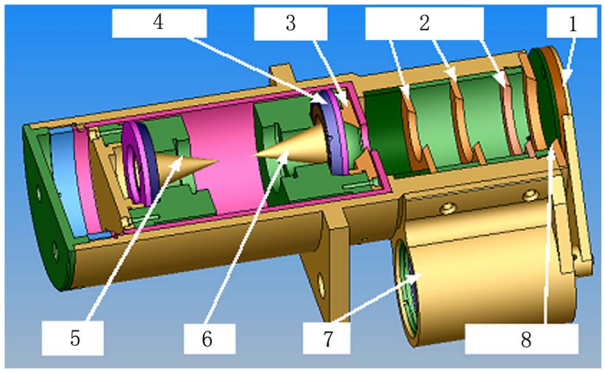

Fig. 1. Schematic of the absolute radiometer SIAR-1a: (1) shutter, (2) apertures for view-limiting, (3) primary aperture, (4) thermocouple ring, (5) reference cavity, (6) primary cavity, (7) motor, and (8) heat sink.

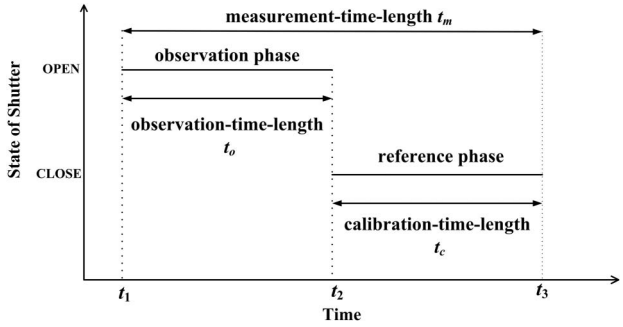

Fig. 2. Illustration of the measurement parameters for a single TSI measurement.

TSI is measured once in two subsequent phases as shown in Fig. 2 [3–6]. The two phases are observation phase and reference phase. The observation phase is from time t_1 to t_2 and the reference phase is from t_2 to t_3. Observation time length t_o, calibration time length t_c, and measurement time length t_m are illustrated in Fig. 2.

In the observation phase, the shutter of the absolute radiometer is open and sunlight is allowed to fall into the primary cavity. As the radiant energy of the incoming sunlight is absorbed by the primary cavity, the heating voltage for the primary cavity is reduced. The temperature feedback provided by the thermocouples of the primary cavity stabilizes at T_{do} at the end of the observation phase.

In the reference phase, the shutter is closed and the heating voltage is determined carefully to make the temperature provided by the thermocouples of the primary cavity stable at T_{do} again. As the electrical power in the two phases can be measured precisely, an accurate measurement of TSI is obtained as follows:

$$E = \frac{u_r^2 - u_o^2}{R_h \cdot A \cdot \alpha}, \tag{1}$$

where E is the total irradiance of the incoming sunlight, u_o is the heating voltage in the observation phase, u_r is the heating voltage in the reference phase, R_h is the heater windings' resistance of the primary cavity, A is the area of the primary aperture, and α is the absorption coefficient of the primary cavity.

3. Thermal Model of the Absolute Radiometer

In this section, it is assumed that the temperature of the heat sink is constant. It is true for radiometers with a temperature control system for the heat sink, such as AR1/TSIM and AR2/TSIM. Considering the

shutter of the absolute radiometer is closed and the primary cavity is only heated by constant electrical power, the thermal dynamics of the absolute radiometer is modeled as below:

$$C\frac{\mathrm{d}T_c(t)}{\mathrm{d}t}+\frac{T_c(t)-T_h(t)}{R_c}+P_{\mathrm{rcs}}+P_{\mathrm{ac}}=P_e+P_{\mathrm{rsc}}, \quad (2)$$

where C is the heat capacity of the primary cavity, $T_c(t)$ is the instantaneous temperature of the primary cavity at time t, R_c is the thermal resistance between the primary cavity and the heat sink, $T_h(t)$ is the instantaneous temperature of the heat sink at time t, P_{rcs} is the radiative power emitted by the primary cavity to the shutter, P_{ac} is the air conduction power transferred from the primary cavity to various regions of the absolute radiometer, P_e is the electrical power applied to the primary cavity, and P_{rsc} is radiative power transferred from the shutter to the primary cavity.

According to Planck's law, the heat radiation exchange between the primary cavity and the shutter is given by

$$\begin{aligned}P_{\mathrm{rcs}}-P_{\mathrm{rsc}}&=\int_0^{2\pi}\int_0^{\omega_h}\left(\frac{\sigma\varepsilon T_c^4}{\pi}-\frac{\sigma\varepsilon T_s^4}{\pi}\right)\cos\theta\,\sin\theta\mathrm{d}\theta\mathrm{d}\varphi\\&=(\sigma T_c^4-\sigma T_s^4)\sin^2\omega_h, \quad (3)\end{aligned}$$

where T_{s} is the temperature of the shutter, σ is Stefan–Boltzmann constant ($\sigma = 5.670 \times 10^{-8}$ $\mathrm{Wm^{-2}K^{-4}}$), $\varepsilon = 1$ represents the emittance for the primary cavity and the shutter, and ω_h is the half-field-of-view of the absolute radiometer.

Air conductance power P_{ac} is given by

$$P_{\mathrm{ac}}=K_a(T_c(t)-T_h(t)), \quad (4)$$

where K_a is air conductance.

Let $T_d(t)$ is the temperature difference between the primary cavity and the heat sink:

$$T_d(t)=T_c(t)-T_h(t). \quad (5)$$

Compiling Eqs. (2)–(5), we obtain

$$C\frac{\mathrm{d}T_d}{\mathrm{d}t}+\frac{T_d}{R}=P, \quad (6)$$

where P is composition heating power and R is thermal resistance:

$$P=P_e-(\sigma T_c^4-\sigma T_s^4)\sin^2\omega_h, \quad (7)$$

$$R=R_c/(1+K_aR_c). \quad (8)$$

Composition heating power P is assumed to be constant for simplicity. It is nearly the truth if time t is sufficient long in general cases.

Solving Eq. (6), temperature difference $T_d(t)$ is given by

$$T_d(t)=c_1+c_2e^{-\frac{t}{\tau}}, \quad (9)$$

where τ is the time constant, and c_1 and c_2 are constants:

$$\tau=CR, \quad (10)$$

$$c_1=RP. \quad (11)$$

Parameters $\{c_1, c_2, \tau\}$ are the timing parameters.

As time $t \to \infty$, temperature $T_d(t)$ approaches a maximum:

$$\lim_{t\to\infty}T_d(t)=\lim_{t\to\infty}(c_1+c_2e^{-\frac{t}{\tau}})=c_1. \quad (12)$$

The ratio between $T_d(t)$ and $T_d(\infty)$ is introduced as below:

$$r(t)=\frac{T_d(t)}{T_d(\infty)}=\frac{T_d(t)}{c_1}. \quad (13)$$

If the shutter is open for TSI measurement, the thermal model of the absolute radiometer is similar to the model discussed above. However, the terms of heat radiation, heat conduction, etc, will be more complex.

TSI can be measured without knowing $T_d(t)$ exactly on Kelvin scale as illustrated in Eq. (1). It is not necessary to transform the digital signal of temperature $T_d(t)$ to Kelvin scale. The digital feedback of $T_d(t)$ is enough for TSI calibration. Errors will be introduced inevitably with transformation to Kelvin-scale temperature. The digital temperature feedback provided by the A/D converter is given in least significant bit (LSB).

4. Estimation of Timing Parameters

The unknown timing parameters $\{c_1, c_2, \tau\}$ in Eq. (9) are estimated through the following procedures:

(1) The absolute radiometer is set to operate in a testing mode. The shutter is always closed in the testing mode.

(2) A constant voltage is applied to the heater winding of the absolute radiometer for N seconds, equivalent to incoming sunlight with irradiance 1367 $\mathrm{Wm^{-2}}$. Temperature $T_d(t)$ is sampled every 1 s. This step is repeated M times to produce data for optimization.

(3) Timing parameters are estimated by a genetic algorithm (GA) [15–17]. The global optimization scheme is implemented in the following steps:

(3.1) Random initialization

Each individual timing parameter $\{c_1, c_2, \tau\}$ is initialized by a chromosome with binary strings [18]. The chromosome consists of genes. A gene is implemented as bit 0 or 1 in the binary strings. Rather

than starting from a single point in the traditional optimization methods, K individuals $\{c_1, c_2, \tau\}_j$ $(j = 1, 2, \ldots, K)$ are created randomly within the search space. Time constants are estimated roughly using neighborhood samples of $T_d(t)$. Only $T_d(t)$ in a specific time interval is used for the approximation. For a given instant t_n and t_{n+1} $(t_{n+1} > t_n)$, it follows that

$$\tau_a = \frac{t_{n+1} - t_n}{\ln\left[\frac{T_d(t_n) - T_d(N)}{T_d(t_{n+1}) - T_d(N)}\right]}. \tag{14}$$

Without a specific bound on the time constant, the solution may fall into a number of local minima and more computation time would generally be consumed.

(3.2) Fitness evaluation

The survival potential of each individual in the population is determined by calculating their fitness function in this step [19]. In order to minimize the estimation error of the timing parameters, the fitness function is constructed as below:

$$f = \sum_{m=1}^{M} \sum_{n=1}^{N} \left| T_d(t_{mn}) - \left(c_1 + c_2 e^{-\frac{t_{mn}}{\tau}}\right)\right|. \tag{15}$$

The timing parameters are constrained to the following condition:

$$c_1 + c_2 = T_d(t_0), \tag{16}$$

where t_0 is initial time.

(3.3) Selection

In the selection step, K couples are selected randomly from the individuals according to a probability associated to their fitness function. The probability of selection increases with a smaller estimation error of timing parameters.

(3.4) Reproduction

New individuals are produced using the couples produced in the selection step. Random perturbation is introduced into the genes of the new individuals, as in the evolutionary process. Some bits of the new individuals' chromosomes are reversed randomly according to a predetermined probability. The mutation operation is to prevent the search algorithm from converging to the local optimum. The search algorithm then goes to step 3.2 again unless a predefined criterion is satisfied. For example, a maximum number of generations allowed or a minimum variation of the fitness function values is reached.

5. Optimization Results

Population size K is set to 80. The maximum number of generations allowed G is set to 200. A stochastic uniform function is chosen to select couples for the next generation. The minimum variation of the fitness function values is set to 10^{-10}. The lower bound and the upper bound of the time constant are obtained from the approximated time constants. Optimized solutions are returned quickly using a computer program in Matlab using its GA toolbox.

The optimized solutions of the timing parameters are given in Table 1. Optimization results including samples of temperature $T_d(t)$, approximate time constants, and fitness function value are shown in Figs. 3–6. The timing parameters are estimated using the data of three experiments. Estimations of the same parameters are roughly consistent. However, slight differences are detected as shown in Table 1, which may be attributed to changes in testing conditions, such as variations of air flow, temperature, etc. The changes lead to variation of composition power P, etc.

Temperatures are reconstructed from Eq. (9) using the optimized solutions of the timing parameters. The reconstructed temperatures are added to Figs. 3(a)–6(a) for comparison. Good agreement between experimental data and reconstructed temperature has been shown in the figures above. The reconstructed temperature nearly coincides with the experimental temperature finally.

6. Selecting Measurement Parameters for the Comparison Experiments

In this section, the measurement parameters for the comparison experiments are selected carefully using the optimized solutions shown in Table 1. Due to the tight schedule, the measurement parameters were set at small values to produce more opportunities for solar measurements. However, observation time length, etc, should not be much too small. Otherwise, temperature $T_d(t)$ does not remain stable at the end of the observation phase or reference phase, producing TSI measurement errors. The measurement parameters for the comparison experiments for TSIM/FY-3C are set as below:

$$t_c = 120 \text{ s}, \tag{17}$$

$$t_o = 120 \text{ s}. \tag{18}$$

Observation time length t_o is set in the interval $[7\tau, 10\tau]$ for each radiometer. For SIAR-1a, the observation time length is about 9τ. For SIAR-2c, the observation time length is about 9.9τ. For AR1/TSIM, the observation time length is about 8τ. For AR2/TSIM, the observation time length is about 7τ.

From Eq. (1), irradiance E can be rewritten as

$$E = f(u_r, u_o, R_c, A, \alpha) = \frac{u_r^2 - u_o^2}{R \cdot A \cdot \alpha}. \tag{19}$$

Uncertainties produced by observation time length and calibration time length are evaluated using Eq. (19). Since observation time length and calibration time length are not infinite, temperature $T_d(t)$ does not reach its maximum c_1 at the end of the observation phase or reference phase. Thus, heating voltages u_o and u_r do not reach their values when

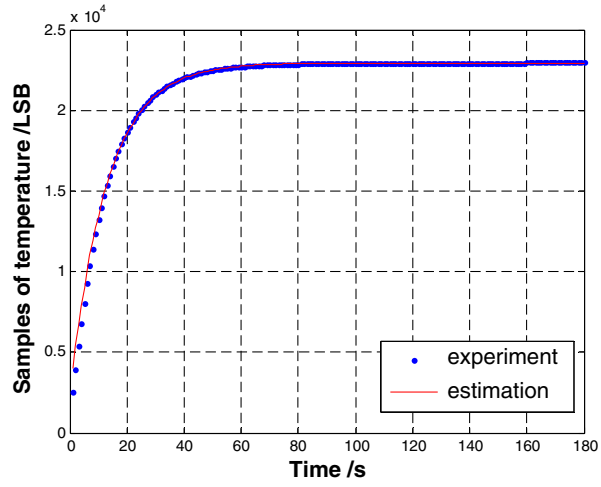

(a)

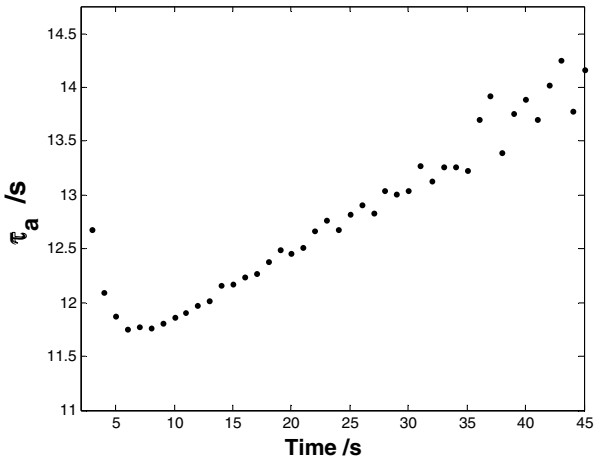

(b)

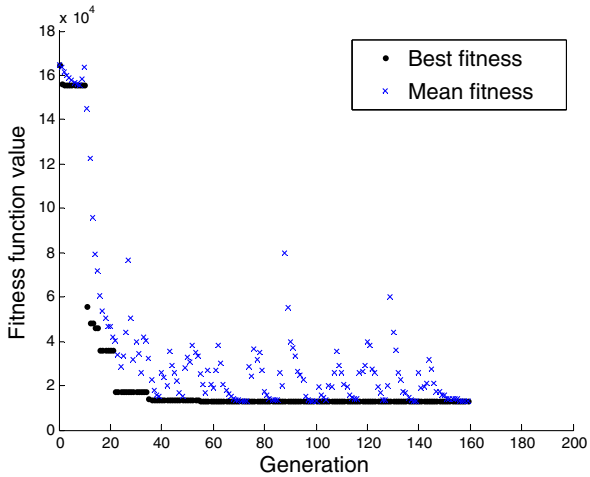

(c)

Fig. 3. Optimization results of SIAR-1a, with data of first experiment given in Table 1. Sampled data of temperature difference $T_d(t)$ are shown in (a) with its estimation for comparison. The reconstructed temperature is obtained from Eq. (9) using optimized solutions of the timing parameters. The bounds of the time constant are obtained from approximate time constants as shown in (b). Fitness function values obtained in the search process of the GA are shown in (c). The GA stops when the minimum variation of the fitness function values is 10^{-10}.

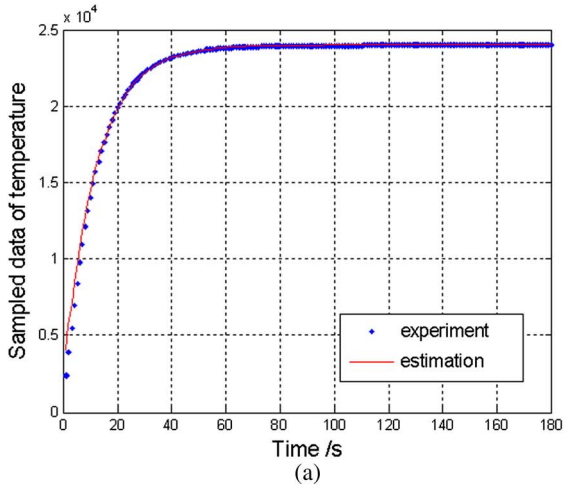

(a)

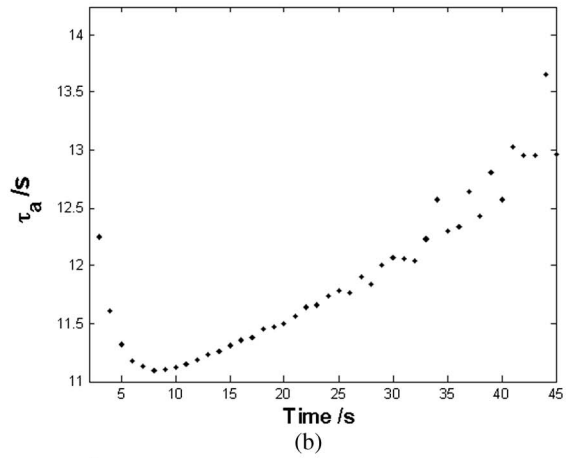

(b)

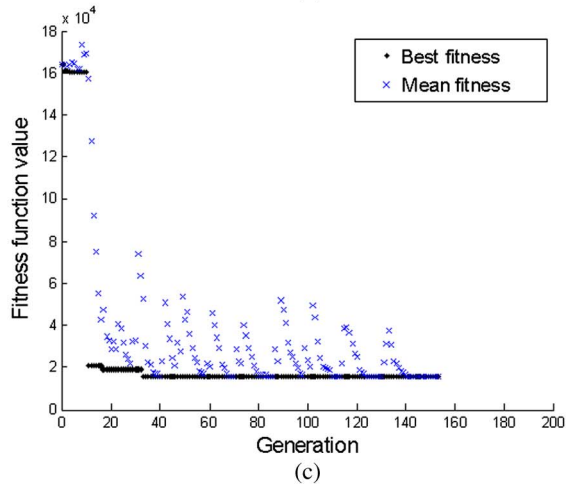

(c)

Fig. 4. Optimization results of SIAR-2c, with data of first experiment given in Table 1. The experimental data of $T_d(t)$ are compared to its estimation constructed using the thermal model of an absolute radiometer and optimized solutions as shown in Table 1. Approximate time constants are presented in (b). Fitness function values by the GA in the search process are shown in (c). The GA stops when the minimum variation of the fitness function values is 10^{-10}.

observation time length and calibration time length are infinite. The standard uncertainty of TSI, produced by observation time length and calibration time length, is given by

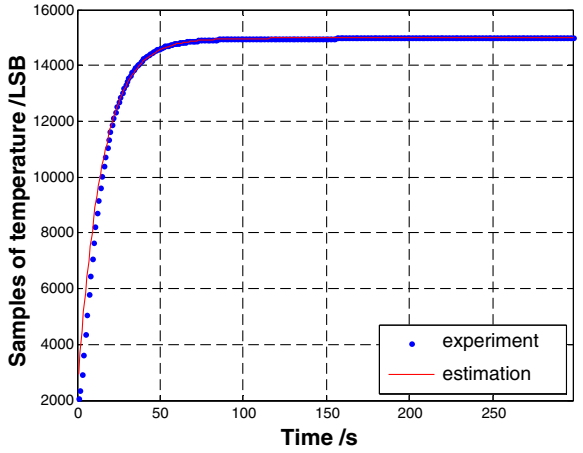

(a)

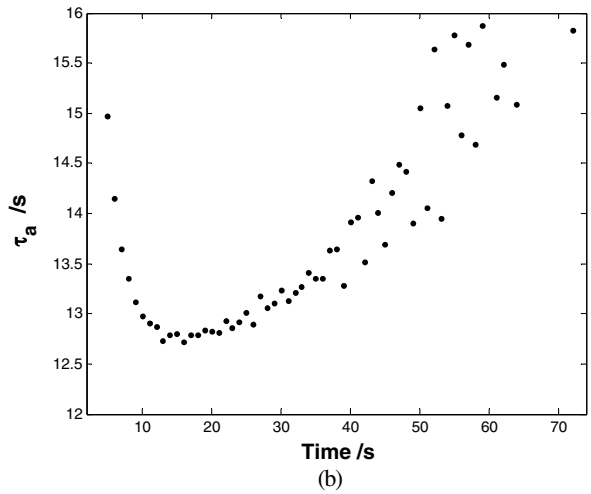

(b)

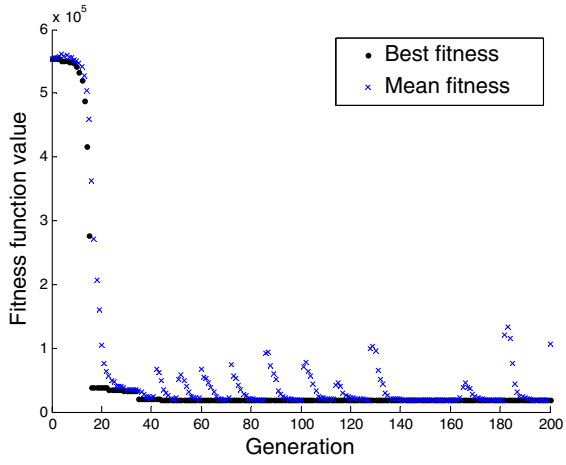

(c)

Fig. 5. Optimization results of AR1/TSIM, with data of first experiment given in Table 1. Temperature difference $T_d(t)$ of the primary cavity is shown in (a). The estimation of temperature $T_d(t)$ is constructed using Eq. (9) and optimized solutions of the timing parameters. The bounds of the time constant are obtained from approximate time constants as shown in (b). Fitness function values by the GA are given in (c). The GA stops when the number of generations is 200.

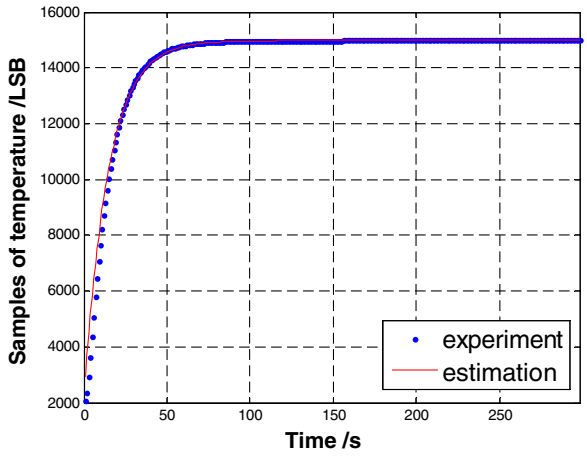

(a)

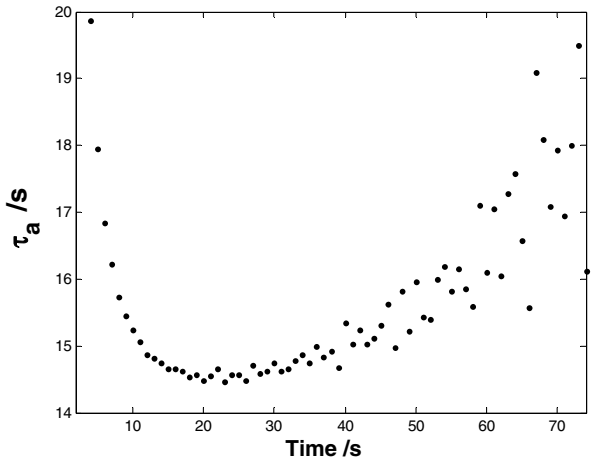

(b)

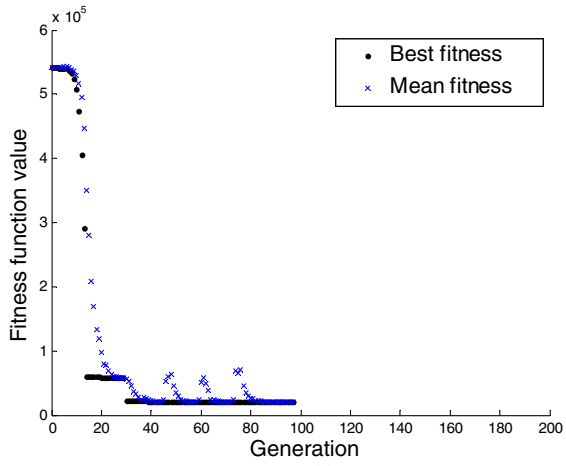

(c)

Fig. 6. Optimization results of AR2/TSIM, with data of first experiment given in Table 1. Sampled data of temperature difference $T_d(t)$ are shown in (a). The estimation of $T_d(t)$ is constructed using the thermal model and optimized solutions of the timing parameters. The estimated temperature is indicated by the solid line, denoted as "estimation" in the legend of (a). Approximate time constants in the specific time interval are shown in (b). Fitness function values by the GA are shown in (c). The GA stops when the minimum variation of the fitness function values is 10^{-10}.

Table 1. Optimization Results of Timing Parameters for Absolute Radiometers

Radiometer	Experiment Number	Time Constant τ	Constant c_1	Constant c_2	Ratio r(120 s)
AR1/TSIM	First	14.5325	14,978.07	−12, 915.07	0.999127
AR1/TSIM	Second	14.5034	14,976.00	−12, 897.00	0.999199
AR1/TSIM	Third	14.5191	14,968.97	−12, 898.97	0.999066
AR2/TSIM	First	16.5097	14,529.00	−12, 548.00	0.998830
AR2/TSIM	Second	16.4771	14,507.00	−12, 519.00	0.998828
AR2/TSIM	Third	16.4950	14,493.96	−12, 516.96	0.998761
SIAR-1a	First	12.9634	22,937.83	−20, 393.83	0.999920
SIAR-1a	Second	13.0454	22,879.06	−20, 389.06	0.999910
SIAR-1a	Third	13.0844	22,869.32	−20, 375.32	0.999942
SIAR-2c	First	12.1407	23,980.94	−21, 586.94	0.999919
SIAR-2c	Second	12.1923	23,852.37	−21, 562.37	0.999900
SIAR-2c	Third	12.2025	23,809.82	−21, 530.82	0.999881

Table 2. TSI Measurement Uncertainty due to Measurement Parameters

Parameter	SIAR-1a	SIAR-2c	AR1/TSIM	AR2/TSIM
A (m^{-2})	5.0027×10^{-5}	5.0987×10^{-5}	5.0290×10^{-5}	5.0300×10^{-5}
R_h (Ω)	847.002	843.640	866.700	855.900
α	0.9997	0.9997	0.9997	0.9997
u_r (V)	7.755	7.695	7.786	7.738
$u(u_r)$ (V)	3.463×10^{-4}	2.949×10^{-4}	3.509×10^{-4}	6.142×10^{-4}
u_o (V)	5.156	5.007	5.119	5.069
$u(u_o)$ (V)	5.075×10^{-4}	4.537×10^{-4}	5.313×10^{-4}	9.332×10^{-4}
E (Wm^{-2})	791.936	793.929	790.070	793.970
Relative uncertainty of E (ppm)	224	188	224	392
$u(E)$ (Wm^{-2})	0.177	0.149	0.177	0.312

$$u^2(E) = \left(\frac{\partial f}{\partial u_r}\right)^2 u^2(u_r) + \left(\frac{\partial f}{\partial u_o}\right)^2 u^2(u_o) = 4\frac{u_r^2 u^2(u_r) + u_o^2 u^2(u_o)}{R_h^2 \cdot A^2 \cdot \alpha^2}, \quad (20)$$

where $u(u_r)$ is the standard uncertainty of voltage u_r and $u(u_o)$ is the standard uncertainty of voltage u_o. $u(u_r)$ and $u(u_o)$ are produced by measurement parameters.

Standard uncertainty $u(E)$ is given in Table 2. Errors introduced by area A, resistance R_c, and absorption coefficient α are not included in Table 2. In addition, heating voltage uncertainties not produced by the measurement parameters for the comparison experiment, such as uncertainties produced by the A/D converter, voltage standard, etc, are not considered in Table 2. AR2's TSI uncertainty is greater than that of other radiometers. It is attributed to that AR2 has a bigger time constant and

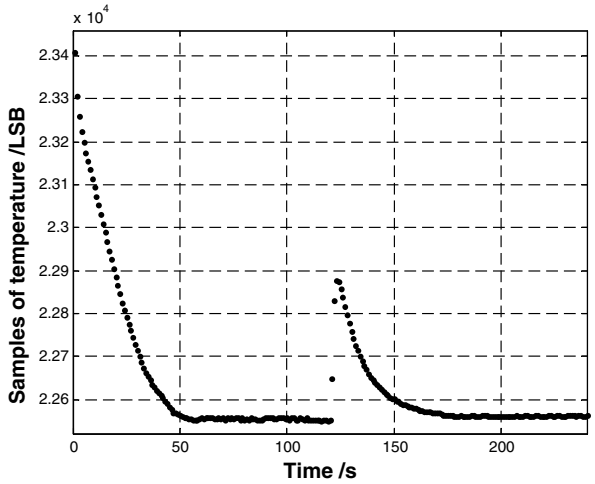

Fig. 7. Samples of temperature $T_d(t)$ for SIAR-1a. The temperature data are obtained in TSI measurement in the comparison experiments.

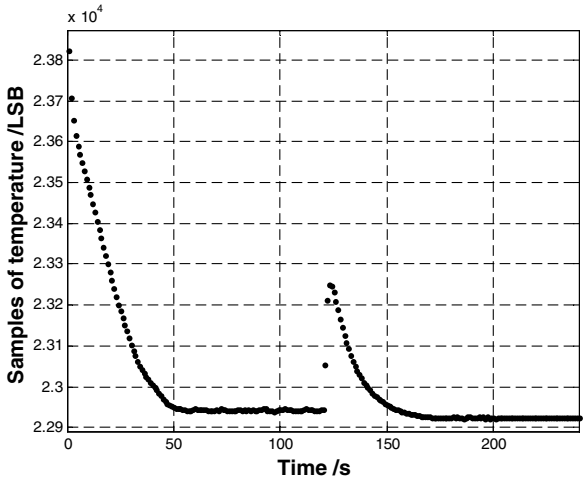

Fig. 8. Samples of temperature $T_d(t)$ for SIAR-2c. The temperature data are obtained in TSI measurement in the comparison experiments.

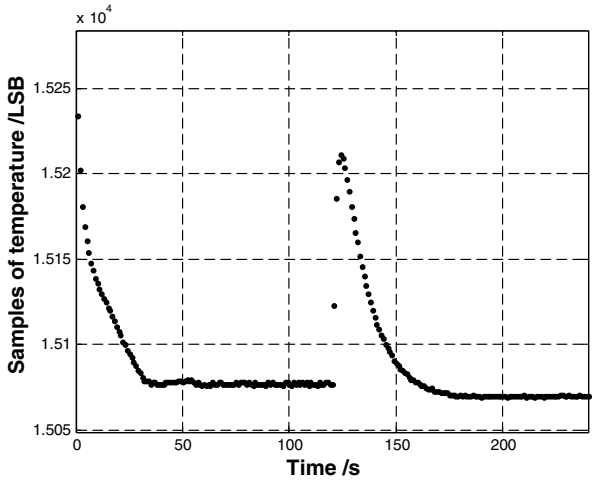

Fig. 9. Samples of temperature $T_d(t)$ for AR1/TSIM. The temperature data are obtained in TSI measurement in the comparison experiments.

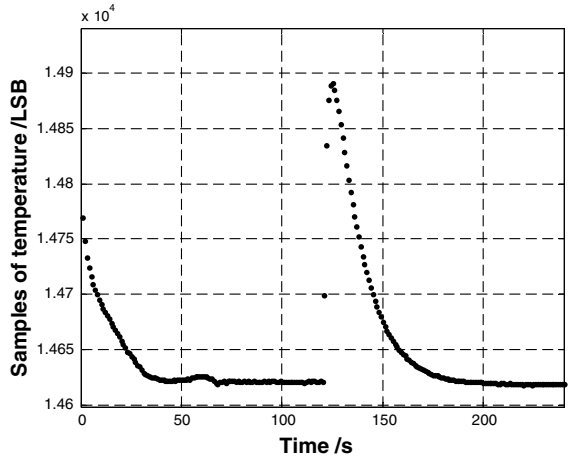

Fig. 10. Samples of temperature $T_d(t)$ for AR2/TSIM. The temperature data are obtained in TSI measurement in the comparison experiments.

smaller r(120 s). Thus, AR2/TSIM is made to work only occasionally in space for studying the degradation of the primary cavity.

As r(120 s) is nearly 0.999 for each radiometer as given in Table 2, the irradiance detected by the cavity sensor is almost the same for each radiometer. Temperature $T_d(t)$ at the end of the observation phase or reference phase is stable for each radiometer using the selected measurement parameters. It is proved by the experimental data in Figs. 7–10. Temperature T_d(120 s) at the end of the observation phase is nearly the same as T_d(240 s) at the end of the reference phase. In summary, the selected measurement parameters are sufficient to produce accurate measurements of TSI.

7. Conclusion

When an electrical substitution radiometer is assembled already for use, an essential step is to properly select measurement parameters, such as observation time length and calibration time length. Accurate measurements of TSI require meaningful selection of the measurement parameters. With plentiful time, the measurement parameters are generally set at high values to get the best measurement accuracy. However, when experiments are performed on a tight schedule, such as the comparison experiments of TSIM/FY-3C, observation time length and calibration time length should be determined carefully to produce more opportunities of solar observation. It is a problem to get a subtle balance of TSI data quality and TSI data quantity. It may be puzzling and time-consuming to select the measurement parameters without knowing the timing parameters of the absolute radiometers. A solution is presented in the paper to solve the selection problem of measurement parameters. An efficient thermal model of an absolute radiometer is proposed to identify the timing parameters, providing the constraints and the objective function for optimization. The model highlights the impact of the timing parameters on the TSI measurement. The timing parameters are searched using a GA to minimize estimation errors. Meaningful selection of measurement parameters is achieved using optimized solutions. Both observation time length and calibration time length are set to 120 s, over the range of $[7\tau, 10\tau]$ for each absolute radiometer. The experimental results indicate that the selection is sufficient to make temperature $T_d(t)$ stable at the end of the observation phase or reference phase. Stable temperature is necessary to calibrate TSI accurately. Compared with TSIM/FY-3B, measurement time length is reduced from 720 to 360 s. It means a shorter time for single TSI measurement, producing more experimental data in a given period. However, observation time length and calibration time length should not be set at too small values. Otherwise, measuring errors will be produced inevitably.

The scheme presented in the paper could be used for applications such as the following: (1) Building a thermal model of some electrical substitution radiometers. (2) Estimating the parameters inside the thermal model. (3) Determining the observation time length and calibration time length for TSI measurement. (4) Uncertainty evaluation of TSI experiments considering errors produced by observation time length and calibration time length. (5) Predicting how fast the cavity detector responds to incoming sunlight, which is important for analysis or test of cavity detectors. For example, choosing specific cavities with similar timing parameters to develop a TSI instrument that consists of multiple absolute radiometers.

The authors thank Baoqi Song, Yupeng Wang, Kai Wang, Xin Ye, Dongjun Yang, etc, for their work. This work is supported by the Development Plan Project for Science and Technology of Jilin Province (No. 20130101044JC) and the Basic Research Project for application of Yunnan Province (No. 2012FD050).

References

1. Z. Yang, N. Lu, J. Shi, P. Zhang, C. Dong, and J. Yang, "Overview of FY-3 payload and ground application system," IEEE Trans. Geosci. Remote Sens. **50**, 4846–4853 (2012).
2. D. Rind, "The sun's role in climate variations," Science **296**, 673–677 (2002).
3. R. C. Willson, "Active cavity radiometer," Appl. Opt. **12**, 810–817 (1973).
4. R. C. Willson, "Active cavity radiometer type IV," Appl. Opt. **18**, 179–188 (1979).
5. R. W. Brusa and C. Fröhlich, "Absolute radiometers (PMO6) and their experimental characterization," Appl. Opt. **25**, 4173–4180 (1986).
6. G. Kopp and G. Lawrence, "The total irradiance monitor (TIM): instrument design," Sol. Phys. **230**, 91–109 (2005).
7. W. Finsterle, "International Pyrheliometer Comparison IPC-XI—Final Report," Technical Report, WMO IOM Report No. 108 (Physikalisch Meteorologisches Observatorium Davos (PMOD)/World Radiation Center (WRC), 2011), 155.
8. G. Kopp, K. Heuerman, and G. Lawrence, "The Total Irradiance Monitor (TIM): instrument calibration," Sol. Phys. **230**, 111–127 (2005).
9. W. Schmutz, A. Fehlmann, G. Hülsen, P. Meindl, R. Winkler, G. Thuillier, P. Blattner, F. Buisson, T. Egorova, W. Finsterle, N. Fox, J. Gröbner, J. Hochedez, S. Koller, M. Meftah, M. Meisonnier, S. Nyeki, D. Pfiffner, H. Roth, E. Rozanov, M. Spescha, C. Wehrli, L. Werner, and J. U. Wyss, "The PREMOS/PICARD instrument calibration," Metrologia **46**, S202–S206 (2009).
10. H. Wang and Y. Wang, "Spaceborne radiometers for measuring total solar irradiance," Chin. Opt. **5**, 555–565 (2012).
11. G. Thuillier, S. Dewitte, and W. Schmutz, "Simultaneous measurement of the total solar irradiance and solar diameter by the PICARD mission," Adv. Space Res. **38**, 1792–1806 (2006).
12. G. Schmidtke, C. Fröhlich, and G. Thuillier, "ISS-SOLAR: total (TSI) and spectral (SSI) irradiance measurements," Adv. Space Res. **37**, 255–264 (2006).
13. H. Wang, Y. Wang, and W. Fang, "Intelligent solar tracker with double modes," Opt. Precision Eng. **19**, 1605–1611 (2011, in Chinese).
14. L. Boivin and F. T. McNeely, "Electrically calibrated absolute radiometer suitable for measurement automation," Appl. Opt. **25**, 554–561 (1986).
15. R. F. Oulton and C. S. Adjiman, "Global optimization and modeling techniques for planar multilayered dielectric structures," Appl. Opt. **45**, 5910–5922 (2006).
16. E. A. Moro, M. D. Todd, and A. D. Puckett, "Using a validated transmission model for the optimization of bundled fiber optic displacement sensors," Appl. Opt. **50**, 6526–6535 (2011).
17. R. A. Taylor, T. Otanicar, and G. Rosengarten, "Nanofluid-based optical filter optimization for PV/T systems," Light **1**, 1–7 (2012).
18. S. P. Poland, A. J. Wright, and J. M. Girkin, "Evaluation of fitness parameters used in an iterative approach to aberration correction in optical sectioning microscopy," Appl. Opt. **47**, 731–736 (2008).
19. P. Kotsidas, E. Chatzi, and V. Modi, "Stationary nonimaging lenses for solar concentration," Appl. Opt. **49**, 5183–5191 (2010).